Rapid Optimization of Metal Nanoparticle Surface Modification with High-Throughput Gel Electrophoresis
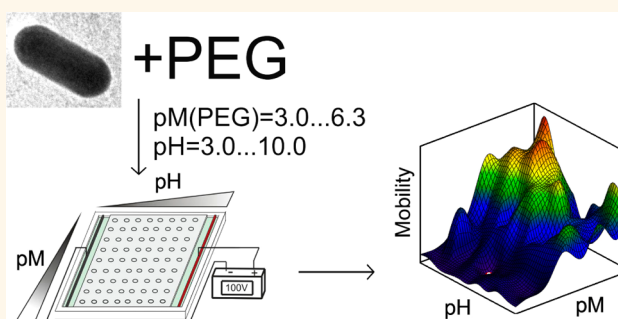
Alexander V. Beskorovaynyy,[†,§] Dmitry S. Kopitsyn,[†,§] Andrei A. Novikov,[†] Maya Ziangirova,[†] Galina S. Skorikova,[†] Mikhail S. Kotelev,[†] Pavel A. Gushchin,[†] Evgeniy V. Ivanov,[†] Michael D. Getmansky,[†] Irving Itzkan,[‡] Alexander V. Muradov,[†] Vladimir A. Vinokurov,[†] and Lev T. Perelman[‡,*]

[†]Center for Nanodiagnostics, Department of Physical and Colloid Chemistry, Gubkin Russian State University of Oil and Gas, Moscow, 119991, Russia and [‡]Center for Advanced Biomedical Imaging and Photonics, Beth Israel Deaconess Medical Center, Harvard University, Boston, Massachusetts 02215, United States. [§]These authors contributed equally.

ABSTRACT The ability to effectively control and optimize surface modification of metal nanoparticles is paramount to the ability to employ metal nanoparticles as diagnostic and therapeutic agents in biology and medicine. Here we present a high-throughput two-dimensional-grid gel electrophoresis cell (2D-GEC)-based method, capable of optimizing the surface modification of as many as 96 samples of metal nanoparticles in approximately 1 h. The 2D-GEC method determines not only the average zeta-potential of the modified particles but also the homogeneity of the surface modification by measuring the distance between the front of the sample track and the area where the maximum optical density is achieved. The method was tested for optimizing pH and concentration of the modifiers (pM) for functionalizing gold nanorod thiol-containing acidic agents.

KEYWORDS: optimization · high-throughput · gel electrophoresis · metal nanoparticles · surface modification · ligand exchange control

D ue to their unique optical properties, gold nanoparticles have lately been widely employed in various biomedical applications, such as gene delivery,[1,2] cell imaging,[3−6] biosensing,[7−10] *in vivo* molecular targeting of cancer cells,[11] photoacoustic imaging in turbid media,[12] *in vivo* SERS spectroscopy,[13] and photothermal therapy.[14,15] The majority of those applications require long-circulating surface-modified nanoparticles with affinity for specific molecular targets. Surface modification of gold nanoparticles is usually performed with bifunctional reagents containing a thiol or dithiol group for chemisorption on a gold surface and a functional group for linking to antibodies or antibiotics. Such reagents include, for example, mercapto-acetic[16] or mercaptobenzoic[17] acids, bifunctional polyethylene glycols (PEG),[18] or alginate-derived polymers.[19] Development of long-circulating target-specific gold nanoparticles[20,21] requires optimization

techniques, which ensure both a high number of attached PEG molecules per surface area and a high surface charge density, which in turn depends on multiple parameters, such as nanoparticle size and size distribution, concentration, temperature, pH, ionic strength, the residual concentration of the stabilizing and replacement surfactants, the duration of the experiment, *etc*. Because each of those parameters can affect the others, the number of mutual combinations of parameters needed to be optimized simultaneously grows exponentially. Up to now, there has been no rapid and inexpensive technique capable of simultaneous optimization of a large number of parameters needed for efficient surface modification of nanoparticles.

A feature of certain types of metal nanoparticles, such as gold nanorods, which is important for biomedical applications, is tunability of the surface plasmon resonance line, facilitating their application for the
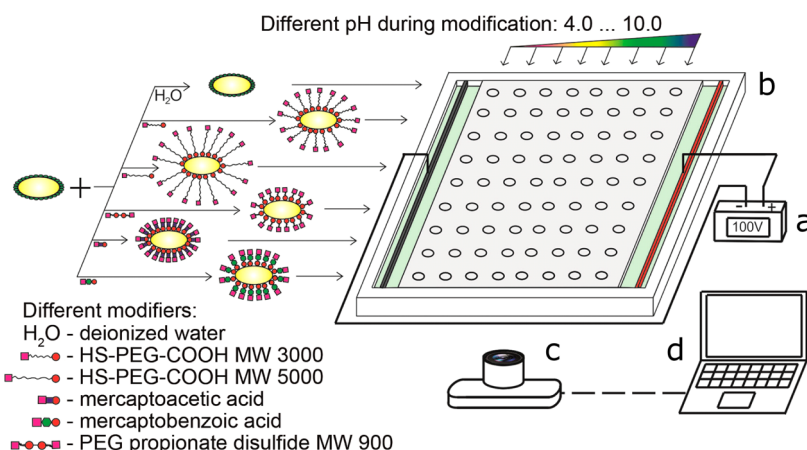
Figure 1. Schematic diagram of the two-dimensional electrophoresis cell-based method: power supply (a), electrophoresis cell (b), digital camera (c), and laptop computer (d).

simultaneous spectroscopic detection of several disease markers[22,23] or for optically selective photothermal therapy.[24] Gold nanorods could be synthesized following standard protocols[25−27] and then tuned to a specific wavelength of the surface plasmon resonance line by selecting proper size and aspect ratio. These size and shape separations could be achieved through rate-zonal centrifugation,[28] ultracentrifugation in a nonhydroxylic organic density gradient,[29] formation of reversible flocculates by surfactant micelle-induced depletion interaction,[30] size exclusion chromatography,[31] field-flow fractionation,[32] employment of recyclable supramolecular membranes,[33] or gel electrophoresis.[34,35] The latter technique requires surface modification under optimal conditions to achieve high particle mobility.

Modern techniques of optimizing parameters of surface modification of the nanoparticles employ mass spectrometry,[36,37] fluorescence spectroscopy,[38] surface plasmon resonance (SPR) technique,[39] dynamic light scattering (DLS),[40] and gel electrophoresis.[41,42] However, except for the gel electrophoresis, a common disadvantage of the above techniques is their inability to control the homogeneity of the reaction for the different particles in the same sample. Not only is gel electrophoresis unaffected by this problem, but it has a very high throughput. In recent publications, the throughput of as many as 13 samples analyzed simultaneously in 30−60 min has been demonstrated.[34,41−43] However, the linear arrangement of the samples in the gel in those studies restricts the number of the simultaneously tested samples to a relatively small number. At the same time, since the nanoparticles' mobility can be evaluated using relatively short tracks, the samples in the gel can be arranged not in a linear fashion but in a two-dimensional grid. This arrangement allows almost unlimited increase in the number of the simultaneously tested samples, which is facilitated even more by the dense

placement of the samples, due to the decrease in the length of the tracks needed for optimization. Thus, the two-dimensional-grid gel electrophoresis arrangement dramatically reduces the per sample optimization time.

In this paper, we describe a high-throughput two-dimensional-grid gel electrophoresis cell (2D-GEC)-based method, capable of optimizing surface modification of a practically unlimited number of samples in a rapid parallel fashion. Moreover, since at least two optimization parameters are varied in the same gel, potential errors related to the variability in the gel properties are removed from the equation. In addition, random errors associated with variability in the experiment duration, voltage, ambient temperature, *etc*. are substantially reduced.

RESULTS AND DISCUSSION

The 2D-GEC setup consisted of the custom-built two-dimensional-grid gel electrophoresis cell, high-current power supply (Bio-Rad PowerPac 164−5052), digital camera, and laptop computer. The schematic diagram of the 2D-GEC method is presented in Figure 1. The two-dimensional-grid gel electrophoresis cell was custom-built from polymethylmethacrylate parts, cut from sheet material and combined by autocured methylmethacrylate glue. Electrodes were cut from stainless steel.

The proposed 2D-GEC method is demonstrated and tested in this paper by optimizing the pH and concentration of the thiol-containing modifiers (pM) for functionalizing gold nanorod thiol-containing acidic agents (mercaptobenzoic acid, mercaptoacetic acid, bifunctional polyethyleneglycoles: PEG propionate disulfide MW 900, HS-PEG-COOH MW 3000 and MW 5000). The gold nanorod samples were synthesized according to the protocol proposed by Sau and Murphy.[44] Briefly, 0.25 mL of 0.01 M tetrachloroauric(III) acid solution and 7.5 mL of 0.1 M CTAB solution were mixed in a capped

soda lime glass tube prewashed with aqua regia and rinsed with deionized water. The 0.6 mL of ice cold 0.01 M sodium tetraborohydride solution was then added to the resulting yellowish-brown solution, and the tube was vigorously shaken for 2 min. The obtained seed solution was left in a 25 °C water bath, and the growth solution was prepared by mixing the appropriate amounts of tetrachloroauric(III) acid, CTAB, ascorbic acid, and silver nitrate solutions. The seed solution and growth solution were mixed and left for 3 h at the ambient temperature. The effective hydrodynamic radius of the gold nanorods was then measured using the DLS technique (Malvern Instruments Zetasizer Nano ZS90) and appeared to be 24.2 nm.

Then the solution was centrifuged for 10 min at 14 100g, the supernatant discarded, and the gold nanorod pellet resuspended in 1.0 mL of modification reagent solution and 0.10 mL of universal buffer solution (acetate-phosphate-borate 120 mM with a pH in the range of 4 to 10). The modification reagent solution was prepared by dissolving mercaptoacetic acid, mercaptobenzoic acid, PEG propionate disulfide, or HS-PEG-COOH in the deionized water. After 2 h, the nanorods were once again centrifuged under the same conditions, resuspended in Tris-borate buffer, and centrifuged again.

The nanorod sample was mixed with 20 μL of glycerol and loaded in the 1.0% agarose gel prepared with 25 mM of Tris-borate buffer. For clarity, the nanorods samples were arranged on the gel so that different rows in the cell were modified with different modifiers while different columns were modified at different values of pH. Electrophoresis was performed at 7.4 V/cm, and running buffer was 2.5 mM Tris-borate.

In the first set of experiments, 36 samples with nanorods modified with HS-PEG-COOH MW 3000, HS-PEG-COOH MW 5000, PEG propionate disulfide MW 900, mercaptoacetic acid, mercaptobenzoic acid, along with unmodified nanorods were loaded in the two-dimensional electrophoresis cell. Simultaneously, the pH was varied from 4.0 to 10.0. The duration of the electrophoresis was 30 min when the digital image of the cell was collected and sent to the control computer to be analyzed by the NIH ImageJ image processing algorithm.[45]

The photograph of the 2D-GEC cell after the electrophoresis is presented in Figure 2. From the length of the tracks (see for example Figure 2c), one can determine the optimal values of the pH for each of the modifiers. Indeed, as can be seen in Figure 2d, the electrophoretic mobility of the modified gold nanoparticles not only strongly depends on the pH of the medium in which the modification was performed but also reaches a maximum at different values of the pH for different modifiers. For example, for mercaptoacetic acid, maximum electrophoretic mobility is
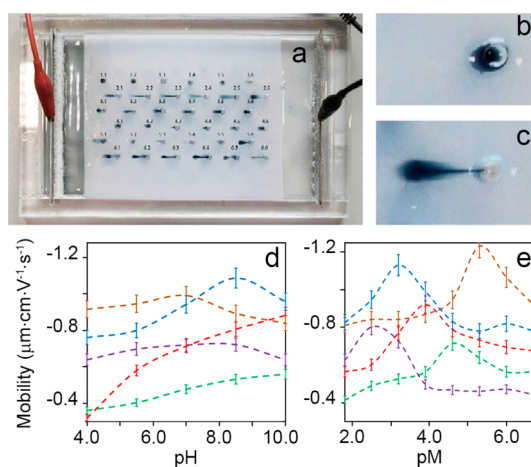

Figure 2. Photograph of the 2D-GEC cell after electrophoresis (a). First row, unmodified nanoparticles; second row, nanoparticles modified with HS-PEG-COOH MW 3000; third row, with HS-PEG-COOH MW 5000; fourth row, with PEG propionate disulfide MW 900; fifth row, with mercaptoacetic acid; and sixth row, with mercaptobenzoic acid. Here, the value of pH is varied over the columns. Sample number 2.6 before (b) and after electrophoresis (c). Dependence of the electrophoretic mobility of the modified gold nanoparticles on the pH of the medium, in which the modification was performed (d). Dependence of the electrophoretic mobility on the pM at the optimum value of pH of the medium during modification (e). Red line, mercaptoacetic acid; brown line, mercaptobenzoic acid; green line, PEG propionate disulfide; blue line, HS-PEG-COOH MW 3000; violet line, HS-PEG-COOH MW 5000.

reached at pH 7.0, while for mercaptobenzoic acid, maximum is reached at pH 8.5.

After establishing the optimum values of the pH, we fixed those pH values and performed the second experiment to optimize the pM (analogous to pH, the value of pM is defined as pM = $-\log_{10}(C_{mod})$, where C_{mod} is a dimensionless parameter, equal to the modifier concentration divided by 1 M) in the reaction medium. The results of these studies are presented in Figure 2e and show that the optimum concentrations of the modifiers vary significantly from modifier to modifier. While for HS-PEG-COOH MW 3000, MW 5000, and mercaptoacetic acid the number of attached PEG molecules per surface area reaches a maximum in the relatively concentrated solutions ($10^{-2}-10^{-3}$ M), for mercaptobenzoic acid and PEG propionate disulfide, the modification maximum is reached in the relatively dilute solutions ($10^{-4}-10^{-5}$ M). We also should note that the method allows evaluating the homogeneity of the surface modification by measuring the distance between the front edge of the sample track and the point where the maximal optical density is achieved. For instance, by analyzing the photograph presented in Figure 2a, one can determine that the highest homogeneity of the surface modification is achieved for the nanoparticles modified with mercaptobenzoic acid.

The dimensions of the custom-built gel electrophoresis cell (Figure 2a) allow testing of a significantly larger
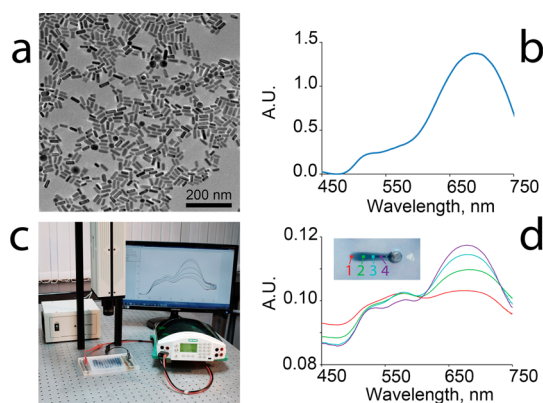
Figure 3. TEM micrograph (a) and typical absorption spectrum (b) of gold nanorods before the surface modification. Photograph of 2D-GEC setup, employing the acousto-optic hyperspectral imaging detector (Gooch & Housego HSi-440C). The absorption spectra from every point on the electrophoresis cell can be shown on the computer screen in real time during the experiment (c). The absorption spectra from the different zones of the electrophoretic track of gold nanorods after surface modification, in the wavelength range from 450 to 750 nm (the inset shows the electrophoretic track) (d).

number of samples than in the first set of experiments. In the second set of experiments, we simultaneously optimized 96 samples in the two-parameter space. Moreover, the 2D-GEC method allows a straightforward combination of electrophoretic mobility testing and the monitoring of the modified nanoparticles' optical spectroscopic characteristics. To demonstrate this, we replaced the standard digital camera employed in the first set of experiments with the acousto-optic hyperspectral imaging detector (Gooch & Housego HSi-440C). This detector collects images of the electrophoresis cell in multiple wavelength regions and provides high-spectral resolution information for each of the tracks of the cell. The photograph of this setup and the absorption spectra from different zones of the electrophoretic track of gold nanorods after surface modification are presented in Figure 3.

To demonstrate the optimization of the gold nanorod surface modification in two-parameter space, we designed an experiment with 96 samples, with the pH of the reaction medium and the concentration of the selected modifier (HS-PEG-COOH MW 3000) varied along two directions of the 2D-GEC cell. The rest of the optimization conditions were similar to the conditions of the first set of experiments.

The pseudocolor map of the electrophoretic mobility of the surface-modified gold nanorods as a function of the pH and pM is presented in Figure 4a with the corresponding 3D plot presented in Figure 4b. It is important to note that since the change of one parameter can affect optimization in other parameters, the map provides important information not available in the regular single-parameter electrophoretic mobility graphs. Indeed, the experiments allowed identifying
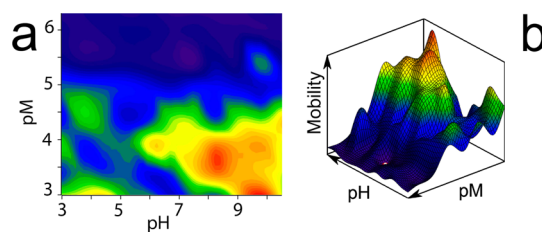

Figure 4. Pseudocolor map (a) and 3D plot (b) of the electrophoretic mobility as a function of the pH and the concentration of the modifier pM. Electrophoretic mobility color codes: blue, less than 0.8 $\mu m \cdot cm \cdot V^{-1} \cdot s^{-1}$; green, 0.8−1.0 $\mu m \cdot cm \cdot V^{-1} \cdot s^{-1}$; yellow, 1.0−1.2 $\mu m \cdot cm \cdot V^{-1} \cdot s^{-1}$; orange, 1.2−1.4 $\mu m \cdot cm \cdot V^{-1} \cdot s^{-1}$; red, more than 1.4 $\mu m \cdot cm \cdot V^{-1} \cdot s^{-1}$.

the pH/pM combination, resulting in 1.52 $\mu m \cdot cm \cdot V^{-1} \cdot s^{-1}$ maximal electrophoretic mobility, a significantly higher value than the results obtained in two successive single-parameter optimization experiments described above when the pH was optimized first and pM second.

Using data on electrophoretic mobility obtained in those experiments and estimating the effective radius of gold nanorods, a, we can now assess the effectiveness of the surface modification at the optimal values of pH = 9.75 and a modifier concentration pM of 3 for PEG3000.

When estimating a, we should note that the DLS-based commercial zeta potentiometers assume a spherical shape for nanoparticles and as a result fail to produce consistent and accurate estimates for gold nanorods.[46] Moreover, they are also inaccurate when taking the flexible polymer tethers into account. Thus to estimate a value of a for gold nanorods, we employed TEM data to evaluate the mean length and mean width of the nanorods's gold core and then adjusted those dimensions by adding the thickness of the PEG layer. As the PEG confirmation in our experiments is not known beforehand, we estimated the PEG layer thickness lower limit (for mushroom conformation) and upper limit (for maximum reach conformation) following Flory's approach outlined by Hanauer et al.[34] and Jeppesen et al.[47] In the case of the mushroom conformation, PEG layer thickness is $h = N^{0.64}l$, where N is the number of the monomer units and $l = 0.35$ nm is the length of the PEG monomer unit. In case of the maximum reach conformation, PEG layer thickness h is calculated from the binding range curve, provided by Jeppesen et al.[47] in Figure 2b. For PEG3000, $h = 5.1$ nm for mushroom conformation and $h = 16.0$ nm for maximum reach conformation. From here, we can find that the effective radius of PEGylated gold nanorods equals 12.8 nm for mushroom PEG conformation and 19.3 nm for maximum reach conformation.

Calculating the Debye length $\kappa^{-1} = (\varepsilon_r \varepsilon_0 k_B T/(2N_A e^2 I))^{1/2}$ for Tris-borate buffer with the ionic strength $I = 25$ mol/m^3, we find $\kappa^{-1} = 1.95$ nm, where

TABLE 1. PEGylated Gold Nanorod Parameters[a]

parameter	bare gold nanorods	gold nanorods with PEG in mushroom conformation	gold nanorods with PEG in maximum reach conformation
mean length, nm	33.0 ± 7.6	38.1 ± 7.6	49.0 ± 7.6
mean width, nm	12.0 ± 2.1	17.1 ± 2.1	28.0 ± 2.1
a, nm	9.6 ± 1.8	12.8 ± 1.8	19.3 ± 1.8
κa	4.9 ± 0.9	6.6 ± 0.9	9.9 ± 0.9
$f(\kappa a)$ (sphere)	0.77 ± 0.02	0.79 ± 0.02	0.84 ± 0.02
$f(\kappa a)$ (cylinder)	0.72 ± 0.02	0.76 ± 0.02	0.82 ± 0.02
ζ, mV (sphere)		-23.8 ± 1.5	-22.6 ± 1.5
ζ, mV (cylinder)		-24.9 ± 1.5	-23.1 ± 1.5
σ, C/m^2		-0.011 ± 0.001	-0.0095 ± 0.001
Γ, PEG/nm^2		0.10 ± 0.01	0.43 ± 0.03

[a] Mean length and mean width of the bare gold nanorods are experimentally measured. The remainder of the parameters are calculated.

ε_r is the relative permittivity, ε_0 is the vacuum permittivity, k_B is the Boltzmann constant, T is the temperature, N_A is the Avogadro number, and e is the elementary charge. This gives the κa parameter equal to 6.6 for mushroom PEG conformation and 9.9 for maximum reach conformation.

To find the zeta-potential of PEGylated gold nanorods, ζ, we can employ Henry's formula[48] for electrophoretic mobility $\mu = \varepsilon_r \varepsilon_0 \eta^{-1} \zeta f(\kappa a)$, where η is the viscosity of water. Here $f(\kappa a)$ is Henry's function, which can be evaluated using the following expression

$$f(\kappa a) = \frac{n-1}{n}$$
$$\times \left[1 + \frac{1}{n-1} \frac{1}{(1 + \delta/\kappa a(1 + (n-1)\cdot \exp(-\kappa a))^{-1})^n} \right] \quad (1)$$

which provides the Ohshima approximations[49,50] for spherical particles if $n = 3$ and $\delta = 2.5$ and randomly oriented infinite cylinders if $n = 2$ and $\delta = 2.55$. Interestingly enough for particles with a κa parameter between 5 and 10, both the spherical particle and randomly oriented infinite cylinder approximations have very similar values. Therefore, we used the mean of these two values for our calculations.

The apparent electrophoretic mobility of PEGylated gold nanorods at the optimal conditions, obtained in the 2D-GEC experiment, is -3.25 cm/h at an electric field strength of 7.4 V/cm. By taking into account the electro-osmotic flow (EOF), we can now calculate the specific mobility of nanorods at optimal conditions. For that, we measured the apparent electrophoretic mobility of a vitamin B12 solution (0.8 cm/h) in the same experiment. As the molecules of vitamin B12 are uncharged, the corresponding value of vitamin B12 specific mobility of 0.30 $\mu m \cdot cm \cdot V^{-1} \cdot s^{-1}$ should be subtracted from the nanorods' specific mobility, which finally gives $\mu = -1.52$ $\mu m \cdot cm \cdot V^{-1} \cdot s^{-1}$.

Knowing the value of the κa parameter, we find the zeta-potential to be in the -22.6 to -24.8 mV range (see Table 1 for details). Since the absolute value of the zeta-potential is close to $k_B T/e \simeq 25.7$ mV while
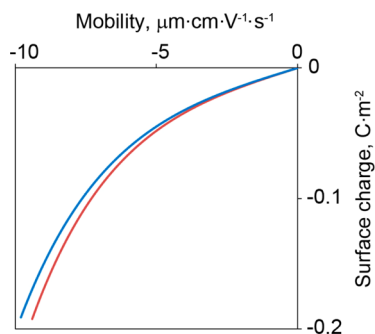

Figure 5. Surface charge density calculated using two approximations of Henry's function at $\kappa a = 6.55$: spherical particle (blue line) and randomly oriented infinite cylinder (red line).

$\kappa a \geq 0.5$, the surface charge density can be calculated using the following expression[51]

$$\sigma = \frac{\varepsilon_r \varepsilon_0 k_B T}{ze} \kappa \left[2\sinh\left(\frac{\zeta ze}{2k_B T}\right) + \frac{4}{\kappa a}\tanh\left(\frac{\zeta ze}{4k_B T}\right) \right] \quad (2)$$

where z is the electrolyte valence.

Surface charge densities, calculated using eq 2 both for the spherical particle and randomly oriented infinite cylinder approximations of Henry's function, are presented in Figure 5 and are very close to each other.

From here, assuming that zeta-potential of the PEGylated gold nanorods is determined entirely by the charge of the PEG carboxyl groups, we can estimate the number of PEG molecules attached per surface area. The dissociation constant pK_a of the PEG-COOH groups is equal to 5.3.[50] At the optimal values of pH = 9.75 and pM(PEG3000) = 3.0, the degree of dissociation of the carboxyl group [COO$^-$]/[COOH] = K_a/[H$^+$] = $10^{-5.3}/10^{-9.75}$ = 28 000, which means that all PEG3000 carboxyl groups are ionized. Taking into account the correction factor, due to the Darcy friction force, caused by the permeability of PEG shell to cations, provided by Doane et al.,[52] the number of PEG molecules attached per surface area is equal to 0.10 PEG/nm^2 for PEG in mushroom conformation and 0.43 PEG/nm^2 in maximum reach conformation. These

values are higher than 0.03−0.05 PEG/nm^2 reported recently for gold nanorods by Xia *et al.*[37] and 0.03−0.07 PEG/nm^2 reported by Pierrat *et al.*[53]

Thus, the 2D-GEC method not only significantly increases the number of simultaneously tested samples and substantially reduces testing time per sample, but also, due to its ability to test several interdependent parameters of optimization simultaneously, can rapidly find a combination of parameters maximizing the number of PEG molecules attached per surface area.

We should note that while cases of high mobility, which are abundant in our experiments, are obviously not affected by agglomeration, in some situations, low mobility could mean agglomeration. At the same time, for practical purposes, this situation should be considered an unsuccessful modification and as such will not affect the determination of the optimal conditions of the modification.

In addition to optimizing the surface modification conditions, the gel electrophoresis of nanoparticles can also be employed for efficient removal of the surfactants and CTAB from gold nanorods. For example, CTAB is often used during synthesis to prevent nanoparticle agglomeration. However, CTAB-capped gold nanorods are almost immediately cleared from the blood circulation with limited distribution to liver, spleen, and lung and no distribution to kidney, heart, thymus, brain, and testes.[20] At the same time, when residual CTAB is removed during regular gel electrophoresis, the agglomeration of nanoparticles often occurs, resulting in the wavelength shift of the surface plasmon resonance peak position or even smearing of the entire spectrum. The 2D-GEC setup with a hyperspectral imaging detector described in this paper allows monitoring of the nanoparticles' spectra during gel electrophoresis experiment. This can lead to the optimization of the CTAB removal parameters, finding the conditions when agglomeration of the nanoparticles is minimized, and ensuring that spectroscopic properties of the nanoparticles are preserved.

CONCLUSION

To summarize the ability to effectively control and optimize surface modification of metal nanoparticles is paramount to be able to employ metal nanoparticles as diagnostic and therapeutic agents in biology and medicine. The high-throughput 2D-GEC gel electrophoresis technique presented in this paper provides rapid optimization of the surface modification of nanoparticles needed to ensure their biocompatibility and selective targeting. The method also allows determining the homogeneity of the surface modification by measuring the distance between the front of the sample track and the area where the maximum optical density is achieved. Finally, the analysis of a large number of samples in the same gel at the same time eliminates the potential errors, associated with the preparation of the gel and the electrophoresis conditions.

METHODS

Materials. Tetrachloroauric(III) acid, cetyltrimethylammonium bromide (CTAB), sodium tetraborohydride, silver nitrate, PEG propionate disulfide, mercaptobenzoic acid, and mercaptoacetic acid were obtained from Sigma-Aldrich; HS-PEG-COOH (MW 3000 and 5000) were acquired from Iris Biotech GmbH; low EEO agarose was purchased from Applichem. Water was deionized in the Vodoley-M system (Himelektronika) and degassed under argon. Analytical grade salts were used for buffer solution preparation. Buffer stock solutions used were Tris-borate 125 mM, pH = 8.8, and universal acetate-phosphate-borate 120 mM, pH = 4−10.

Nanoparticle Surface Modification. The gold nanorods suspension (1.0 mL) was centrifuged using a MiniSpinPlus centrifuge (Eppendorf) for 10 min at 14 100*g*. After the supernatant was discarded, the gold nanorod pellet was resuspended in 1.0 mL of the modifier solution and 0.10 mL of universal buffer solution with various pH. The modifier solution was prepared by dissolving mercaptoacetic acid, mercaptobenzoic acid, PEG propionate disulfide, or HS-PEG-COOH in the deionized water. After 2 h, the nanorods were centrifuged again for 10 min at 14 100*g*, resuspended in Tris-borate buffer, and centrifuged once again under the same conditions. The obtained pellet was mixed with 20 μL of glycerol, and the resulting sample was loaded on the agarose gel.

Agarose Gel Preparation. For gel preparation, 2.0 g of agarose, 8.0 mL of 125 mM Tris-borate buffer solution, and 242 mL of distilled water were boiled in a glass beaker covered by a watch glass until all the agarose was dissolved.

Electrophoresis Cell Construction. The cell was manufactured from polymethylmethacrylate parts cut from sheet material and combined by autocured methylmethacrylate glue; the electrodes were cut from stainless steel.

REFERENCES AND NOTES

1. Salem, A. K.; Searson, P. C.; Leong, K. W. Multifunctional Nanorods for Gene Delivery. *Nat. Mater.* **2003**, *2*, 668−671.
2. Chen, C. C.; Lin, Y. P.; Wang, C. W.; Tzeng, H. C.; Wu, C. H.; Chen, Y. C.; Chen, C. P.; Chen, L. C.; Wu, Y. C. DNA-Gold Nanorod Conjugates for Remote Control of Localized Gene Expression by Near Infrared Irradiation. *J. Am. Chem. Soc.* **2006**, *128*, 3709−3715.
3. Durr, N. J.; Larson, T.; Smith, D. K.; Korgel, B. A.; Sokolov, K.; Ben-Yakar, A. Two-Photon Luminescence Imaging of Cancer Cells Using Molecularly Targeted Gold Nanorods. *Nano Lett.* **2007**, *7*, 941−945.
4. Eghtedari, M.; Oraevsky, A.; Copland, J. A.; Kotov, N. A.; Conjusteau, A.; Motamedi, M. High Sensitivity of *In Vivo*

Detection of Gold Nanorods Using a Laser Optoacoustic Imaging System. *Nano Lett.* **2007**, *7*, 1914–1918.

5. Huang, X.; El-Sayed, I. H.; Qian, W.; El-Sayed, M. A. Cancer Cell Imaging and Photothermal Therapy in the Near-Infrared Region by Using Gold Nanorods. *J. Am. Chem. Soc.* **2006**, *128*, 2115–2120.

6. El-Sayed, I. H.; Huang, X.; El-Sayed, M. A. Surface Plasmon Resonance Scattering and Absorption of Anti-EGFR Antibody Conjugated Gold Nanoparticles in Cancer Diagnostics: Applications in Oral Cancer. *Nano Lett.* **2005**, *5*, 829–834.

7. Bauer, L. A.; Birenbaum, N. S.; Meyer, G. J. Biological Applications of High Aspect Ratio Nanoparticles. *J. Mater. Chem.* **2004**, *14*, 517–526.

8. He, W.; Huang, C. Z.; Li, Y. F.; Xie, J. P.; Yang, R. G.; Zhou, P. F.; Wang, J. One-Step Label-Free Optical Genosensing System for Sequence-Specific DNA Related to the Human Immunodeficiency Virus Based on the Measurements of Light Scattering Signals of Gold Nanorods. *Anal. Chem.* **2008**, *80*, 8424–8430.

9. Sudeep, P. K.; Joseph, S. T.; Thomas, K. G. Selective Detection of Cysteine and Glutathione Using Gold Nanorods. *J. Am. Chem. Soc.* **2005**, *127*, 6516–6517.

10. Yu, C.; Varghese, L.; Irudayaraj, J. Surface Modification of Cetyltrimethylammonium Bromide-Capped Gold Nanorods To Make Molecular Probes. *Langmuir* **2007**, *23*, 9114–9119.

11. Eghtedari, M.; Liopo, A. V.; Copland, J. A.; Oraevsky, A. A.; Motamedi, M. Engineering of Hetero-functional Gold Nanorods for the *In Vivo* Molecular Targeting of Breast Cancer Cells. *Nano Lett.* **2009**, *9*, 287–291.

12. Funke, A. R.; Bossy, E.; Aubry, J.-F.; Fink, M.; Boccara, A.-C. Selective Ultrasonic Focusing towards an Optical Contrast Agent by Use of Photoacoustic-Guided Time-Reversal. *J. Acoust. Soc. Am.* **2008**, *123*, 3640–3640.

13. Kneipp, J.; Kneipp, H.; Wittig, B.; Kneipp, K. Novel Optical Nanosensors for Probing and Imaging Live Cells. *Nanomedicine* **2010**, *6*, 214–226.

14. Norman, R. S.; Stone, J. W.; Gole, A.; Murphy, C. J.; Sabo-Attwood, T. L. Targeted Photothermal Lysis of the Pathogenic Bacteria, *Pseudomonas aeruginosa*, with Gold Nanorods. *Nano Lett.* **2008**, *8*, 302–306.

15. Kawano, T.; Niidome, Y.; Mori, T.; Katayama, Y.; Niidome, T. PNIPAM Gel-Coated Gold Nanorods for Targeted Delivery Responding to a Near-Infrared Laser. *Bioconjugate Chem.* **2009**, *20*, 209–212.

16. Li, J. L.; Wang, L.; Liu, X. Y.; Zhang, Z. P.; Guo, H. C.; Liu, W. M.; Tang, S. H. *In Vitro* Cancer Cell Imaging and Therapy Using Transferrin-Conjugated Gold Nanoparticles. *Cancer Lett.* **2009**, *274*, 319–326.

17. Ackerson, C. J.; Jadzinsky, P. D.; Sexton, J. Z.; Bushnell, D. A.; Kornberg, R. D. Synthesis and Bioconjugation of 2 and 3 nm-Diameter Gold Nanoparticles. *Bioconjugate Chem.* **2010**, *21*, 214–218.

18. Mei, B. C.; Oh, E.; Susumu, K.; Farrell, D.; Mountziaris, T. J.; Mattoussi, H. Effects of Ligand Coordination Number and Surface Curvature on the Stability of Gold Nanoparticles in Aqueous Solutions. *Langmuir* **2009**, *25*, 10604–10611.

19. Kodiyan, A.; Silva, E. A.; Kim, J.; Aizenberg, M.; Mooney, D. J. Surface Modification with Alginate-Derived Polymers for Stable, Protein-Repellent, Long-Circulating Gold Nanoparticles. *ACS Nano* **2012**, *6*, 4796–4805.

20. Lankveld, D. P.; Rayavarapu, R. G.; Krystek, P.; Oomen, A. G.; Verharen, H. W.; van Leeuwen, T. G.; De Jong, W. H.; Manohar, S. Blood Clearance and Tissue Distribution of PEGylated and Non-PEGylated Gold Nanorods after Intravenous Administration in Rats. *Nanomedicine* **2011**, *6*, 339–349.

21. Kim, B.; Han, G.; Toley, B. J.; Kim, C. K.; Rotello, V. M.; Forbes, N. S. Tuning Payload Delivery in Tumour Cylindroids Using Gold Nanoparticles. *Nat. Nanotechnol.* **2010**, *5*, 465–472.

22. Qiu, L.; Larson, T. A.; Vitkin, E.; Guo, L.; Hanlon, E. B.; Itzkan, I.; Sokolov, K. V.; Perelman, L. T. Gold Nanorod Light Scattering Labels for Biomedical Imaging. *Biomed. Opt. Express* **2010**, *1*, 135–142.

23. Huang, H.; Liu, F.; Huang, S.; Yuan, S.; Liao, B.; Yi, S.; Zeng, Y.; Chu, P. K. Sensitive and Simultaneous Detection of Different Disease Markers Using Multiplexed Gold Nanorods. *Anal. Chim. Acta* **2012**, *755*, 108–114.

24. Wang, Y.; Black, K. C.; Luehmann, H. P.; Li, W.; Zhang, Y.; Cai, X.; Wan, D.; Liu, S.-Y.; Li, M.; Kim, P.; *et al.* A Comparison Study of Gold Nanohexapods, Nanorods, and Nanocages for Photothermal Cancer Treatment. *ACS Nano* **2013**, *7*, 2068–2077.

25. Huang, B. X.; Neretina, S.; El-Sayed, M. A. Gold Nanorods: From Synthesis and Properties to Biological and Biomedical Applications. *Adv. Mater.* **2009**, *21*, 1–31.

26. Smith, D. K.; Korgel, B. A. The Importance of the CTAB Surfactant on the Colloidal Seed-Mediated Synthesis of Gold Nanorods. *Langmuir* **2008**, *24*, 644–649.

27. Ye, X.; Jin, L.; Caglayan, H.; Chen, J.; Xing, G.; Zheng, C.; Doan-Nguyen, V.; Kang, Y.; Engheta, N.; Kagan, C. R.; *et al.* Improved Size-Tunable Synthesis of Monodisperse Gold Nanorods through the Use of Aromatic Additives. *ACS Nano* **2012**, *6*, 2804–2817.

28. Akbulut, O.; Mace, C. R.; Martinez, R. V.; Kumar, A. A.; Nie, Z.; Patton, M. R.; Whitesides, G. M. Separation of Nanoparticles in Aqueous Multiphase Systems through Centrifugation. *Nano Lett.* **2012**, *12*, 4060–4064.

29. Bai, L.; Ma, X.; Liu, J.; Sun, X.; Zhao, D.; Evans, D. G. Rapid Separation and Purification of Nanoparticles in Organic Density Gradients. *J. Am. Chem. Soc.* **2010**, *132*, 2333–2337.

30. Park, K.; Koerner, H.; Vaia, R. A. Depletion-Induced Shape and Size Selection of Gold Nanoparticles. *Nano Lett.* **2010**, *10*, 1433–1439.

31. Knoppe, S.; Boudon, J.; Dolamic, I.; Dass, A.; Bürgi, T. Size Exclusion Chromatography for Semipreparative Scale Separation of $Au_{38}(SR)_{24}$ and $Au_{40}(SR)_{24}$ and Larger Clusters. *Anal. Chem.* **2011**, *83*, 5056–5061.

32. Schmidt, B.; Loeschner, K.; Hadrup, N.; Mortensen, A.; Sloth, J. J.; Bender Koch, C.; Larsen, E. H. Quantitative Characterization of Gold Nanoparticles by Field-Flow Fractionation Coupled Online with Light Scattering Detection and Inductively Coupled Plasma Mass Spectrometry. *Anal. Chem.* **2011**, *83*, 2461–2468.

33. Krieg, E.; Weissman, H.; Shirman, E.; Shimoni, E.; Rybtchinski, B. A Recyclable Supramolecular Membrane for Size-Selective Separation of Nanoparticles. *Nat. Nanotechnol.* **2011**, *6*, 141–146.

34. Hanauer, M.; Pierrat, S.; Zins, I.; Lots, A.; Sonnichsen, C. Separation of Nanoparticles by Gel Electrophoresis According to Size and Shape. *Nano Lett.* **2007**, *7*, 2881–2885.

35. Xu, X.; Caswell, K. K.; Tucker, E.; Kabisatpathy, S.; Brodhacker, K. L.; Scrivens, W. A. Size and Shape Separation of Gold Nanoparticles with Preparative Gel Electrophoresis. *J. Chromatogr. A* **2007**, *1167*, 35–41.

36. Hinterwirth, H.; Kappel, S.; Waitz, T.; Prohaska, T.; Lindner, W.; Lämmerhofer, M. Quantifying Thiol Ligand Density of Self-Assembled Monolayers on Gold Nanoparticles by Inductively Coupled Plasma Mass Spectrometry. *ACS Nano* **2013**, *7*, 1129–1136.

37. Xia, X.; Yang, M.; Wang, Y.; Zheng, Y.; Li, Q.; Chen, J.; Xia, Y. Quantifying the Coverage Density of Poly(ethylene glycol) Chains on the Surface of Gold Nanostructures. *ACS Nano* **2012**, *6*, 512–522.

38. Liu, Y.; Shipton, M. K.; Ryan, J.; Kaufman, E. D.; Franzen, S.; Feldheim, D. L. Synthesis, Stability, and Cellular Internalization of Gold Nanoparticles Containing Mixed Peptide-Poly(ethylene glycol) Monolayers. *Anal. Chem.* **2007**, *79*, 2221–2229.

39. Ma, Y.; Chechik, V. Aging of Gold Nanoparticles: Ligand Exchange with Disulfides. *Langmuir* **2011**, *27*, 14432–14437.

40. Song, W. J.; Du, J. Z.; Sun, T. M.; Zhang, P. Z.; Wang, J. Gold Nanoparticles Capped with Polyethyleneimine for Enhanced siRNA Delivery. *Small* **2010**, *6*, 239–246.

41. Sperling, R. A.; Pellegrino, T.; Li, J. K.; Chang, W. H.; Parak, W. J. Electrophoretic Separation of Nanoparticles with a Discrete Number of Functional Groups. *Adv. Funct. Mater.* **2006**, *16*, 943–948.

42. Bartczak, D.; Kanaras, A. G. Preparation of Peptide-Functionalized Gold Nanoparticles Using One Pot EDC/Sulfo-NHS Coupling. *Langmuir* **2011**, *27*, 10119–10123.

43. Perrault, S. D.; Chan, W. C. Synthesis and Surface Modification of Highly Monodispersed, Spherical Gold Nanoparticles of 50−200 nm. *J. Am. Chem. Soc.* **2009**, *131*, 17042–17043.

44. Sau, T. K.; Murphy, C. J. Seeded High Yield Synthesis of Short Au Nanorods in Aqueous Solution. *Langmuir* **2004**, *20*, 6414–6420.

45. Schneider, C. A.; Rasband, W. S.; Eliceiri, K. W. NIH Image to ImageJ: 25 Years of Image Analysis. *Nat. Methods* **2012**, *9*, 671–675.

46. Park, S.; Sinha, N.; Hamad-Schifferli, K. Effective Size and Zeta Potential of Nanorods by Ferguson Analysis. *Langmuir* **2010**, *26*, 13071–13075.

47. Jeppesen, C.; Wong, J. Y.; Kuhl, T. L.; Israelachvili, J. N.; Mullah, N.; Zalipsky, S.; Marques, C. M. Impact of Polymer Tether Length on Multiple Ligand-Receptor Bond Formation. *Science* **2001**, *293*, 465–468.

48. Henry, D. C. The Cataphoresis of Suspended Particles. Part I. The Equation of Cataphoresis. *Proc. R. Soc. A* **1931**, *133*, 106–129.

49. Ohshima, H. A Simple Expression for Henry's Function for the Retardation Effect in Electrophoresis of Spherical Colloidal Particles. *J. Colloid Interface Sci.* **1994**, *168*, 269–271.

50. Ohshima, H. Henry's Function for Electrophoresis of a Cylindrical Colloidal Particle. *J. Colloid Interface Sci.* **1996**, *180*, 299–301.

51. Emoto, K.; Van Alstine, J. M.; Harris, J. M. Stability of Poly(ethylene glycol) Graft Coatings. *Langmuir* **1998**, *14*, 2722–2729.

52. Doane, T. L.; Chuang, C. H.; Hill, R. J.; Burda, C. Nanoparticle ζ-Potentials. *Acc. Chem. Res.* **2012**, *45*, 317–326.

53. Pierrat, S.; Zins, I.; Breivogel, A.; Sönnichsen, C. Self-Assembly of Small Gold Colloids with Functionalized Gold Nanorods. *Nano Lett.* **2007**, *7*, 259–263.